การศึกษาในหุ่นจำลองเพื่อประเมินประสิทธิภาพของเทคนิค Iterative Metal Artifact Reduction (iMAR) ในงานรังสีรักษาระยะไกล

Impact of iterative Metal Artifact Reduction (iMAR) on External Beam Radiotherapy: A Phantom Sttudy

ศันสนีย คงคุ้ม[1], พิชญุตม์ นาคกระแสร์[1], พลอย ดังสมัคร[1]

[1]สาขาวิชารังสีรักษา ภาควิชารังสีวิทยา คณะแพทยศาสตร์ศิริราชพยาบาล มหาวิทยาลัยมหิดล

ผู้นิพนธ์ประสานงาน

พลอย ดังสมัคร

สาขาวิชารังสีรักษา ภาควิชารังสีวิทยา คณะแพทยศาสตร์ศิริราชพยาบาล มหาวิทยาลัยมหิดล

2 ถนนวังหลัง แขวงศิริราช เขตบางกอกน้อย กรุงเทพมหานคร ประเทศไทย 10700

อีเมล : ploy.dan@mahidol.ac.th

Sansanee Kongkum[1], Pitchayut Nakkrasae[1], Ploy Dangsamak[1]

[1]Division of Radiation Oncology, Department of Radiology, Faculty of Medicine Siriraj Hospital, Mahidol University, Thailand

Corresponding author

Ploy Dangsamak

Division of Radiation Oncology, Department of Radiology, Faculty of Medicine Siriraj Hospital, Mahidol University

2 Wanglang Road, Siriraj, Bangkok Noi, Bangkok, Thailand, 10700

E-mail: ploy.dan@mahidol.ac.th

Submitted: Mar 16, 2026

Revised: Jun 9, 2026

Accepted: Jun 28, 2026

บทคัดย่อ

หลักการและเหตุผล: โลหะในร่างกายผู้ป่วยส่งผลให้ภาพเอกซเรย์คอมพิวเตอร์ (Computed Tomography; CT) เกิดสัญญาณรบกวนประเภทโลหะ (metallic artifact) นำไปสู่ความคลาดเคลื่อนของความหนาแน่นเนื้อเยื่อ (Hounsfield Unit; HU) ซึ่งส่งผลกระทบความแม่นยำในการคำนวณปริมาณรังสีในงานรังสีรักษาระยะไกล

วัตถุประสงค์: เพื่อศึกษาประสิทธิภาพของอัลกอริทึมการลดสัญญาณรบกวนจากโลหะแบบทำซ้ำ (Iterative Metal Artifact Reduction: iMAR) ต่อความแม่นยำของค่า HU และการคำนวณปริมาณรังสีในหุ่นจำลอง

วัสดุและวิธีการ: ประเมินคุณภาพเครื่อง CT ตามมาตรฐาน AAPM TG-66 ด้วยหุ่นจำลอง Catphan® 600 จากนั้นถ่ายภาพ CT หุ่นจำลองชนิด CIRS Gammex Phantom ร่วมกับแท่งเหล็กกล้าคาร์บอน (carbon steel) ที่จำลองสถานการณ์ทางคลินิก เพื่อเปรียบเทียบความถูกต้องของค่า HU ทั้งแบบใช้และไม่ใช้ iMAR นอกจากนั้นการศึกษานี้ยังนำภาพ CT ของหุ่นจำลองชนิด CIRS pelvis phantom มาวางแผนการรักษาด้วยระบบวางแผนการรักษา Eclipse ด้วยโฟตอนพลังงาน 6 และ 10 MV ด้วยสมการคำนวณรังสีแบบ GBBS เพื่อประเมินความถูกต้องของการคำนวณรังสีแบบจุดและวิเคราะห์ค่าดัชนีแกมมา (Gamma index analysis) บนภาพที่ใช้และไม่ใช้ iMAR

ผลการศึกษา: ภาพ CT ผ่านการทดสอบตามเกณฑ์มาตรฐานของ AAPM TG-66 ในการศึกษาด้วยหุ่นจำลองชนิด CIRS Gammex phantom พบว่า Metallic Artifact รบกวนภาพ CT จำนวนมากขึ้นเมื่อเพิ่มแหล่งกำเนิดโลหะ และเทคนิค iMAR ลดสัญญาณรบกวนรวมถึงช่วยเพิ่มความถูกต้องของ HU ในทุกสถานการณ์จำลองทางคลินิก นอกจากนั้นหุ่นจำลองชนิด CIRS pelvis phantom แสดงให้เห็นว่าภาพ CT ที่ผ่านการปรับปรุงด้วย iMAR ช่วยเพิ่มความแม่นยำในการคำนวณรังสีเมื่อเทียบกับภาพที่มีสัญญาณรบกวน โดยช่วยลดเปอร์เซ็นต์ความแตกต่างของปริมาณรังสีแบบจุด (จาก 0.66% เหลือ 0.44% สำหรับ 6 MV และ 1.82% เหลือ 0.64% สำหรับ 10 MV) และปรับปรุงค่าดัชนีแกมมาโดยเฉพาะที่ระดับ 2%/2 มม. ที่เพิ่มขึ้นจากประมาณ 87–89 เปอร์เซ็นต์ (ไม่ใช้ iMAR) มาเป็น 97 เปอร์เซ็นต์ (ใช้ iMAR) แต่ไม่พบความแตกต่างที่ระดับ 3%/3 มม. จากการใช้และไม่ใช้ iMAR

ข้อสรุป: เทคนิค iMAR ช่วยลดสัญญาณรบกวนจากโลหะและทำให้อ่านค่า HU ได้แม่นยำ ซึ่งจำเป็นต่อการวางแผนรังสีรักษาระยะไกล ช่วยให้คำนวณปริมาณรังสีได้ถูกต้องตามจริงและเหมาะสมต่อแผนการรักษาภายใต้เกณฑ์ทางคลินิกที่ซับซ้อน

คำสำคัญ: การลดสัญญาณรบกวนจากโลหะแบบทำซ้ำ, ค่าความหนาแน่นของเนื้อเยื่อในหน่วยของภาพเอกซเรย์คอมพิวเตอร์, ความแม่นยำในการคำนวณปริมาณรังสี

Abstract

Background: Metallic implants introduce significant artifacts in computed tomography (CT) images, leading to Hounsfield Unit (HU) inaccuracies and subsequent errors in external beam radiotherapy dose calculations.

Objective: This study evaluated the impact of iterative metal artifact reduction (iMAR) on CT image quality, electron density representation, and dosimetric accuracy using a phantom-based model.

Materials & Methods: Initial CT simulator performance was validated against AAPM Task Group 66 standards using a Catphan® 600 phantom. To assess HU recovery, carbon steel rods were inserted into a CIRS Gammex phantom in various configurations to simulate clinical scenarios (e.g., spinal lesions, prosthetic hips). Images were reconstructed with and without the iMAR algorithm across five smoothness levels. Dosimetric impact was evaluated using a CIRS pelvic phantom and the Eclipse treatment planning system. Dose distributions for 6 MV and 10 MV photon beams were calculated using the Grid-Based Boltzmann Solver (GBBS) algorithm. Accuracy was quantified using point dose comparisons and gamma index analysis.

Results: CT quality assurance confirmed all parameters were within clinical tolerances. In the presence of metal, uncorrected images exhibited severe streaking and photon starvation. However, iMAR significantly restored HU fidelity and anatomical visualization, particularly in complex multi-metal geometries. Dosimetrically, iMAR-corrected datasets yielded point doses closer to the reference data, reducing the percentage dose difference (from 0.66% to 0.44% at 6 MV and 1.82% to 0.64% at 10 MV). While both corrected and uncorrected plans passed the 3%/3 mm gamma criteria (>99%), the stricter 2%/2 mm criteria revealed a substantial decline in uncorrected passing rates (~87–89%). The application of iMAR restored these passing rates to >97% and significantly reduced standard deviation, indicating improved procedural consistency.

Conclusion: The iMAR algorithm effectively mitigates metal-induced artifacts and restores CT number accuracy. Its implementation is critical for high-precision EBRT planning, as it ensures dose calculation stability and superior gamma passing rates under stringent clinical criteria.

Keywords: iterative Metallic artifact reduction (iMAR), Hounsfield unit correction, Dose calculation accuracy

J Thai Assoc Radiat Oncol 2026; 32(2): R1 - R15

Introduction

Metallic implants are increasingly encountered in patients undergoing external beam radiotherapy (EBRT) due to the growing use of prostheses, surgical fixation devices, and dental restorations[1]. Although these implants enhance structural support and quality of life, they pose significant challenges for EBRT planning and delivery by degrading computed tomography (CT) image quality, compromising the accuracy of target delineation and dose calculation[2]. Metal artifacts, which typically manifest as streaks and shadowing, result from the high attenuation of metallic materials, which distort CT numbers or Hounsfield units (HU), leading to inaccuracies in tissue characterization and increased uncertainty in dose distribution[3]. Such distortions can adversely affect EBRT planning accuracy and potentially influence clinical outcomes.

To mitigate metal-induced artifacts, advanced metal artifact reduction (MAR) techniques have been developed, including iterative metal artifact reduction (iMAR), a commercially available sinogram-based algorithm[4]. Unlike conventional filtering approaches, iMAR employs a multi-step iterative process that includes metal segmentation and forward projection, normalized metal artifact reduction (NMAR) (**Figure 1**) using a prior image to replace corrupted sinogram data, and frequency-splitting techniques that preserve high-frequency anatomical detail while suppressing low-frequency streak artifacts[5]. These processes aim to restore CT number fidelity and improve visualization of anatomical structures adjacent to metallic implants, which is particularly critical for radiotherapy planning.

Despite demonstrated improvements in CT image quality, the clinical integration of iMAR into EBRT workflows remains variable, and its quantitative impact on dose calculation accuracy has not been fully established[6]. Phantom studies provide a controlled and reproducible environment for systematically evaluating imaging algorithms without the confounding effects of patient variability. By employing tissue-equivalent phantoms containing metallic inserts, the influence of artifact reduction techniques on CT number accuracy, electron density representation, and dosimetric outcomes can be isolated and assessed[7]. Accordingly, this study investigates the impact of iMAR on EBRT planning using a phantom model, focusing on improvements in CT image quality, accuracy of electron density estimation, and their consequent effects on dose calculation. The findings are expected to inform clinical implementation strategies and support optimization of radiotherapy protocols for patients with metallic implants.

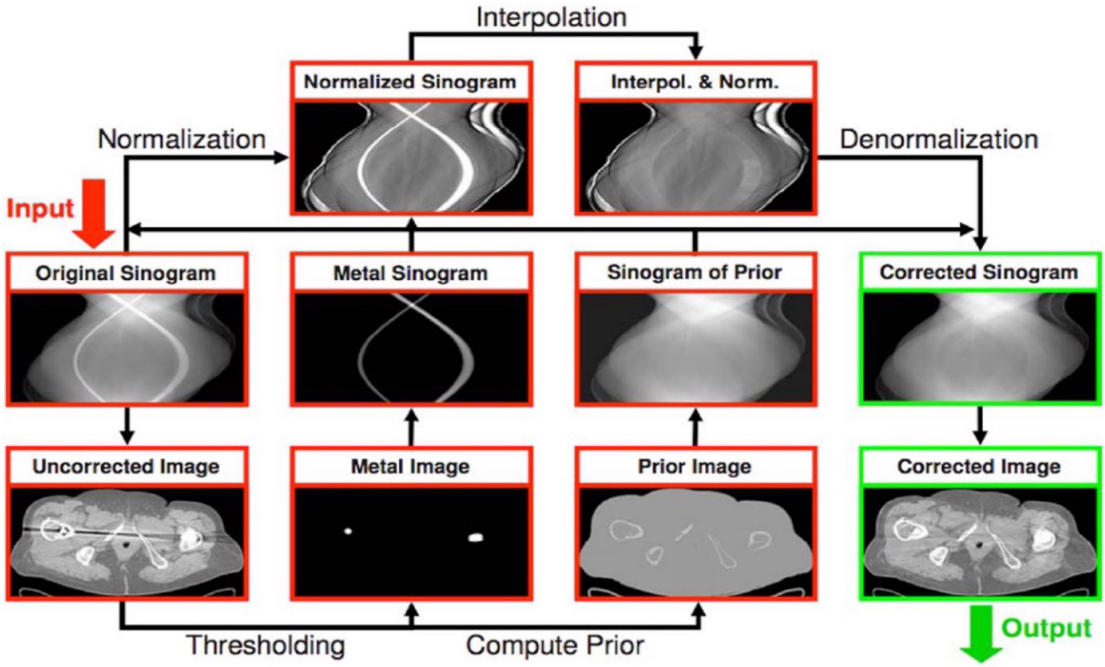


Figure 1. Multi-step iterative process of normalized metal artifact reduction (NMAR)[5]

Materials and methods

CT Image quality assessment

To ensure CT image quality in this study, the Catphan® 600 phantom (The Phantom Laboratory, Salem, NY, USA) underwent CT simulation (SOMATOM Confidence® RT Pro, Siemens Healthineers, Erlangen, Germany) to assess image quality in accordance with AAPM Task Group No. 66 recommendations[8]. Standard CT exposure protocols (120 kVp, 140 mA, field of view 490 mm) with a slice thickness of 3 mm were applied. Image quality metrics evaluated included high spatial resolution, low-contrast detectability, CT number accuracy, uniformity, slice position accuracy, and slice thickness accuracy.

Hounsfield Unit (HU) improvement using iMAR with the CIRS Gammex phantom

The CIRS Gammex phantom model 467 (GAMMEX, Middleton, WI, USA), containing standard tissue-equivalent density rods, underwent CT simulation using standard clinical exposure protocols. The phantom was aligned at the scanner isocenter, and images were reconstructed using routine clinical reconstruction settings. The HU values obtained from this reference scan without metal inserts were

defined as the reference dataset. Each scan was repeated three times under identical conditions to assess measurement reproducibility, and the mean HU values were used for analysis.

Carbon steel rods with a density of 7.849 g/cm³ were subsequently inserted into the phantom under multiple geometric configurations, as illustrated in **Figure 2**, to produce varying degrees of metal-induced artifacts (metallic implant in spinal lesion, metallic implant in prosthetic hip, dental filling metallic artifacts, and multiple metallic implants at different locations). For each scenario, CT images were reconstructed with and without iMAR correction. The iMAR algorithm was applied using five image smoothness levels (iMAR 1 – iMAR 5) to the artifact blurring. Quantitative HU analysis was performed using circular regions of interest with an area of approximately 400 mm² placed within the tissue-equivalent inserts and selected background regions while avoiding visible artifact streaks where possible. The measured HU values for each metal scenario and iMAR smoothness level were compared with the corresponding reference values. HU differences (HU) were calculated and subsequently analyzed.

Impact of iMAR on EBRT dose calculation accuracy: a pelvic phantom study

The CIRS pelvic phantom model 002PRA (CIRS, Norfolk, VA, USA) was scanned under two conditions: (1) without metal inserts and (2) with a carbon steel rod inserted at the hip location to simulate a high-density metallic implant. CT datasets from both conditions were imported into the Eclipse treatment planning system (TPS), version 18.0.1 (Varian Medical Systems, Palo Alto, CA, USA), to generate EBRT treatment plans using identical beam geometry, optimization settings, and calculation parameters, enabling direct comparison of dose distributions. Anteroposterior (AP) fields with both 6 and 10 MV photon beams and a fixed 200 monitor unit (MU) were used to generate the isodose distributions. Dose calculations were performed using the Grid-Based Boltzmann Solver (GBBS) algorithm, which accounts for tissue heterogeneity and radiation transport effects. The dose calculation grid size and heterogeneity correction settings were kept constant for all plans. The same structure set and CT-to-electron density calibration curve were applied consistently across all datasets.

Dose calculation accuracy was evaluated using point dose comparisons and gamma index analysis. Five-point dose differences along the beam axis were assessed at predefined reference locations, as shown in **Figure 3**, within the target volume and selected organs at risk. Gamma analysis was performed using acceptance criteria of 3%/3 mm and 2%/2 mm (%dose difference/distance-to-agreement) in MEPHYSTO Navigator software (PTW, Freiburg, Germany). Gamma passing rates were recorded and compared between scenarios to quantify the impact of metal artifacts and correction methods on EBRT dose calculation accuracy.

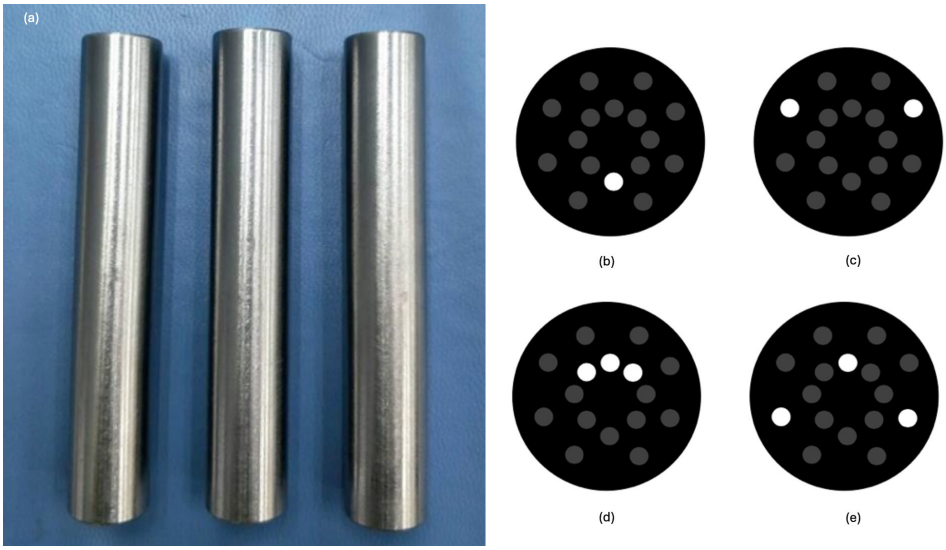


Figure 2. (a) carbon steel rods with a density of 7.849 g/cm³, and different locations to generate different metallic scenarios: (b) metallic implant in spinal lesion, (c) metallic implant in prosthetic hip, (d) dental filling metallic artifacts, and (e) multiple metallic implants at different locations

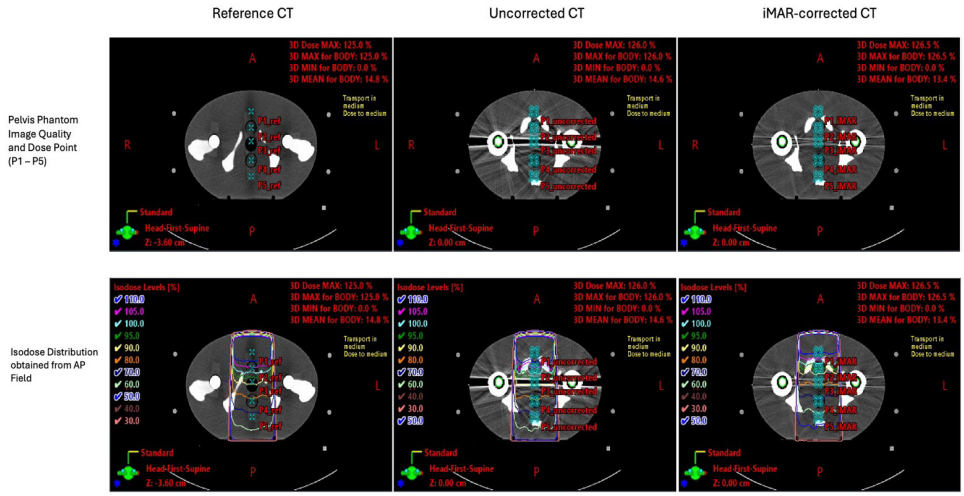


Figure 3. CT data set and isodose comparisons across reference CT, uncorrected- and iMAR-corrected CT

Results

CT image quality assessment

The quality assurance results for the CT simulator are presented in **Table 1**. All evaluated parameters complied with performance criteria specified in AAPM Task Group 66 guidelines, confirming the suitability of the CT simulator for clinical EBRT planning applications.

Hounsfield Unit (HU) improvement using iMAR with the CIRS Gammex phantom

Figure 4 illustrates a comparative performance analysis of the iMAR algorithm across four distinct phantom configurations, labeled (a) through (d), each representing an increasing degree of metal-induced image degradation. In the uncorrected CT, the presence of high-density metal pins triggers severe photon starvation and beam hardening, manifesting as radial streaks and dark bands that obscure the surrounding soft-tissue-equivalent inserts. As the complexity of the metal hardware progresses, from a single pin to a wide triangular distribution, the interference patterns become more pronounced, virtually eliminating the diagnostic utility of the central regions in the uncorrected images.

In our study, the iMAR-corrected images demonstrated a significant restoration of image quality and contrast-to-noise ratio. This correction is particularly vital in scenario Figure 4d, where the previously blacked-out region between the three metal pins is recovered, enabling visualization of nearby structures. This comparison highlights the algorithm's ability to mitigate the non-linear errors inherent in metal-perturbed sinograms, thereby facilitating more accurate volumetric and densitometric assessments in clinical scenarios involving orthopedic or dental implants. The iMAR algorithm effectively suppresses streaking artifacts while preserving morphological integrity and HU consistency as shown in **Figure 5.**

The data are demonstrated in four bar charts, labeled Figure 5(a) – (d), comparing five different levels of iMAR-corrected images (iMAR 1 to iMAR 5) with uncorrected CT data. The y-axis represents the absolute ΔHU values, while the x-axis includes various tissue-equivalent materials and simulated inserts, including cortical bone, adipose tissue, brain, solid water, lung, and liver. Each panel corresponds to a different experimental condition, such as variations in implant material, geometry, or proximity to the metal source, resulting in progressively increasing artifact severity across the figures. Figure 5(a) demonstrates the mildest artifact condition, with ΔHU values peaking at approximately 25 HU, whereas Figures 5(b) and 5(c) exhibit moderate artifact levels. Figure 5(d) represents the most severe scenario, where uncorrected errors increase dramatically to approximately 210 HU. Across all experimental conditions, a consistent trend is observed in which iMAR significantly reduces HU deviations compared with uncorrected images. The uncorrected datasets, represented by the darkest bars, show substantial deviations from the reference baseline. In contrast, all iMAR protocols, represented by lighter gray bars, markedly reduce these distortions and restore ΔHU values toward

Table 1. Image quality test for CT simulator following AAPM TG-66 recommendation

Parameters	Evaluated Criteria	Location	Measurement	Pass/Fail
HU accuracy	± 50 HU	Air (-1000)	-999.85 HU	Pass
		PMP (-200)	-182.2 HU	Pass
		LDPE (-100)	-92.4 HU	Pass
		Polystyrene (-35)	-34.8 HU	Pass
		Acrylic (120)	127 HU	Pass
		Delrin (240)	348 HU	Pass
		Teflon (990)	947.2 HU	Pass
Geometric accuracy	± 1mm	Anterior (50 mm)	50.4 mm	Pass
		Posterior (50 mm)	50.3 mm	Pass
		Left (50 mm)	50 mm	Pass
		Right (50 mm)	50.3 mm	Pass
Slice thickness accuracy	± 1 mm	Setting (3 mm)	2.86 mm	Pass
High contrast resolution	≥ 5-line pair/cm	-	7-line pair/cm	Pass
Low contrast detectability	≤ 4 mm at 1%	Contrast level of supra slice 1%	4 mm	Pass
Uniformity	± 5 HU	#1 Center	6.2 HU	Pass
		#2 Anterior	5.5 HU	Pass
		#3 Left	5.7 HU	Pass
		#4 Posterior	5.9 HU	Pass
		#5 Right	5.5 HU	Pass
		#1 - #5	< 5 HU	Pass

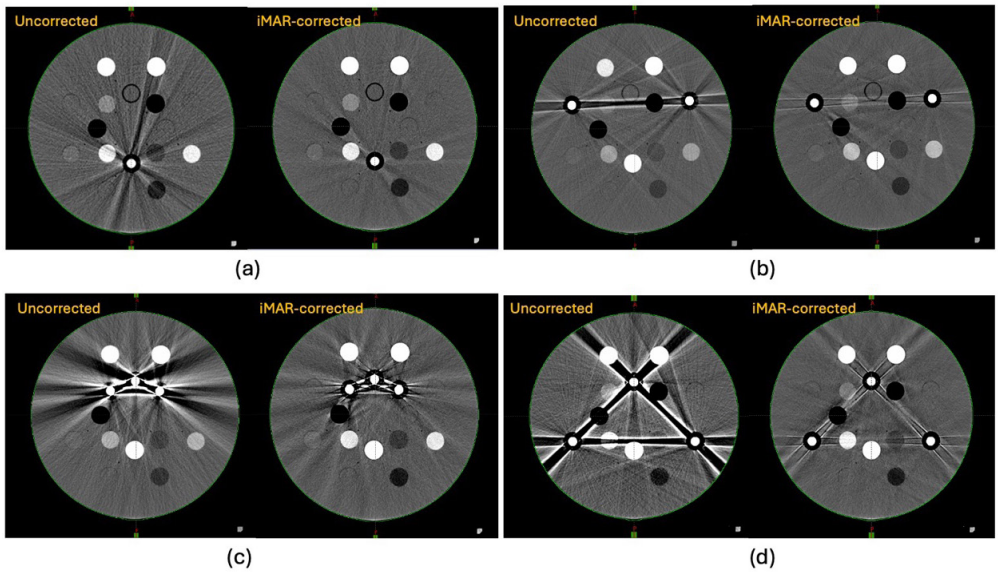


Figure 4. Comparison of uncorrected and iMAR-corrected images in different metallic scenarios: (a) metallic implant in spinal lesion, (b) metallic implant in prosthetic hip, (c) dental filling metallic artifacts, and (d) multiple metallic implants at different locations

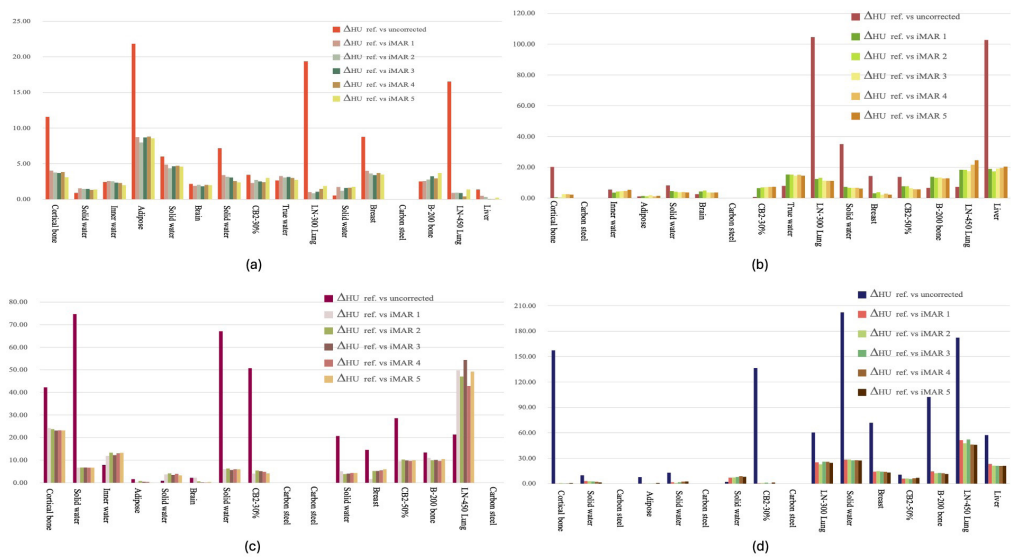


Figure 5. Comparison of the different HU values related to the CT reference image in different metallic scenarios: (a) metallic implant in spinal lesion, (b) metallic implant in prosthetic hip, (c) dental filling metallic artifacts, and (d) multiple metallic implants at different locations

zero, demonstrating the algorithm's effectiveness in recovering CT number accuracy.

Although all iMAR smoothness settings achieved comparable HU accuracy, only minor differences were observed among the various correction levels.

Impact of iMAR on EBRT dose calculation accuracy: a pelvic phantom study

The comparative analysis evaluated the dosimetric impact of the iMAR algorithm on calculated doses for 6 and 10 MV photon beams. The data from **Tables 2 and 3** demonstrate that applying the iMAR correction significantly enhances the accuracy and reliability of dose distributions when compared to uncorrected CT images. In the point dose evaluation across five specific points (P1 – P5), the iMAR-corrected images consistently yielded values closer to the established ground truth than the uncorrected datasets. For instance, at the P2 point for a 10 MV photon beam, the percentage dose difference decreased from 0.44% in the uncorrected image to 0.16% following the iMAR application. While the uncorrected images generally maintained a dose difference below 2%, the iMAR correction provided a more stable dose calculation, minimizing outliers and reducing the relative error across nearly all measured points. Moreover, P1 exhibited a higher percentage dose difference in the iMAR-corrected images (0.76% and 0.66% for 6 and 10 MV, respectively) compared with the uncorrected images (0.26% and 0.14% for 6 and 10 MV, respectively). However, when considering the absolute dose, the variation remained minimal and clinically acceptable.

The most profound improvements were observed in the gamma passing rate analysis, particularly under more stringent criteria. When applying the 3%/3mm gamma criteria, both corrected and uncorrected images performed well, maintaining passing rates above 99%. However, under the 2%/2mm criteria, the uncorrected images showed a significant decline in accuracy, falling to 89.13±10.00% for 6 MV photons and 87.47±1.55% for 10 MV photons. The implementation of iMAR correction restored these passing rates to clinically acceptable levels of 98.33±1.77% and 97.80±2.08%, respectively. Furthermore, the dramatic reduction in standard deviation from double digits to approximately 2% indicates that iMAR not only improves absolute accuracy but also ensures greater procedural consistency. In conclusion, while standard CT imaging may suffice for loose tolerances, the iMAR algorithm is essential for high-precision radiotherapy planning where strict gamma criteria are required to ensure patient safety and treatment efficacy.

Table 2. Comparison of TPS calculated doses (Gy) and percentage dose differences across reference CT, uncorrected CT, and iMAR-corrected CT for 6 MV and 10 MV photon beams

No. of dose point	TPS calculated dose (Gy); mean ± SD			% dose difference	
	reference CT	uncorrected CT	iMAR-corrected CT	reference CT vs uncorrected Image	reference CT vs iMAR-corrected CT
6 MV photon					
- P1	2.200 ± 0.01	2.205 ± 0.010	2.216 ± 0.01	0.26	0.76
- P2	1.896 ± 0.01	1.884 ± 0.013	1.893 ± 0.01	0.62	0.14
- P3	1.655 ± 0.02	1.669 ± 0.167	1.662 ± 0.01	0.66	0.40
- P4	1.349 ± 0.01	1.373 ± 0.01	1.375 ± 0.01	1.95	1.90
- P5	1.124 ± 0.01	1.138 ± 0.01	1.138 ± 0.01	1.28	1.25
10 MV photon					
- P1	2.334 ± 0.01	2.337 ± 0.01	2.349 ± 0.01	0.14	0.66
- P2	2.063 ± 0.02	2.054 ± 0.01	2.060 ± 0.02	0.44	0.16
- P3	1.836 ± 0.02	1.870 ± 0.18	1.848 ± 0.02	1.82	0.64
- P4	1.548 ± 0.01	1.576 ± 0.01	1.576 ± 0.01	1.83	1.85
- P5	1.333 ± 0.01	1.348 ± 0.03	1.348 ± 0.04	1.15	1.13

Table 3. Comparison of mean percentage gamma passing rates for 6 MV and 10 MV photon beams using 3%/3mm and 2%/2mm gamma criteria

Gamma criteria	% gamma passing rate (Mean±SD)	
	reference CT vs uncorrected CT	reference CT vs iMAR-corrected CT
6 MV photon		
- 3%, 3mm	99.83 ± 0.29	99.93 ± 0.12
- 2%, 2mm	89.13 ± 10.00	98.33 ± 1.77
10 MV photon		
- 3%, 3mm	99.67 ± 0.58	99.87 ± 0.23
- 2%, 2mm	87.47 ± 11.55	97.80 ± 2.08

Discussion

CT quality assurance and imaging reliability

To ensure the integrity of the dosimetric analysis, the CT simulator was validated against AAPM Task Group 66 standards[8]. All parameters, from spatial resolution to HU uniformity, remained within tolerance, ensuring the scanner's geometric accuracy (±1 mm) met the strict requirements for EBRT target localization. This high-precision calibration is fundamental for the GBBS algorithm to perform accurate, heterogeneity-corrected dose calculations. Consequently, the study's findings on metal artifact correction can be interpreted without the confounding influence of baseline scanner error.

Effectiveness of iMAR in reducing metal-induced artifacts

Metallic implants are known to produce severe CT artifacts, including streaking and dark bands, primarily due to photon starvation, beam hardening, and scatter effects[5,9]. These artifacts distort HU and compromise anatomical visualization, particularly in regions adjacent to high-density materials. The application of the iMAR algorithm significantly reduced these artifacts by combining metal segmentation, normalized metal artifact reduction (NMAR), and frequency-splitting techniques[5]. In this study, iMAR restored image contrast and improved HU consistency across all phantom configurations, including complex multi-metal scenarios. The ability of iMAR to recover previously obscured regions demonstrates its effectiveness in correcting non-linear sinogram perturbations and improving CT number fidelity[10]. These improvements are clinically important for accurate tissue characterization and contour delineation in EBRT planning.

Dosimetric impact on EBRT planning

Accurate CT number representation is essential for dose calculation algorithms that account for tissue heterogeneity. Metal-induced HU distortions can propagate into electron density errors, thereby affecting dose computation accuracy[11]. In this study, point dose analysis revealed that iMAR reduced percentage dose differences across most evaluation points for both 6 MV and 10 MV photon beams. For example, at point P2 (10 MV), the dose difference decreased from 0.44% to 0.16% after iMAR correction. Although uncorrected dose deviations remained below 2%, iMAR provided more stable and consistent dose estimations. Moreover, the gamma analysis further highlighted the clinical relevance of artifact correction. While both datasets met the 3%/3 mm acceptance criteria (>99% passing rate), the stricter 2%/2 mm criteria revealed significant degradation in uncorrected images (~87–89%). The application of iMAR restored gamma passing rates to above 97% and substantially reduced variability. These findings are consistent with previous investigations demonstrating that MAR techniques improve dose calculation accuracy and reduce uncertainty in high-precision EBRT workflows[10,11].

Clinical implications

Although conventional CT datasets may appear acceptable under standard tolerance levels, stricter quality assurance criteria reveal that metal artifacts introduce clinically relevant variability. The integration of iMAR into routine EBRT workflows may reduce electron density misrepresentation, improve dose calculation stability, enhance gamma passing rates under strict criteria, and minimize reliance on manual density overrides. Given the increasing prevalence of metallic implants in oncology patients, the use of advanced MAR algorithms such as iMAR should be strongly considered, particularly in high-precision EBRT protocols.

Study limitations and future perspectives

The study was conducted using controlled phantom models, a method that strengthens internal validity by eliminating motion and patient-specific anatomical variability. While this approach provides a stable baseline, the researchers emphasize that clinical studies are now required to confirm the magnitude of these benefits within real-world patient datasets. A notable limitation of the current investigation was the exclusive evaluation of carbon steel implants. Because different materials, such as titanium or cobalt-chromium alloys, may produce distinct artifact characteristics, expanding the scope of materials is a primary recommendation for future work.

To build upon these findings, future research should transition into more complex clinical environments. This includes assessing the impact of artifacts in advanced radiotherapy techniques like IMRT and VMAT, as well as evaluating their role in adaptive radiotherapy workflows. Furthermore, there is a clear need to explore the interaction between iMAR and emerging dose calculation algorithms to ensure accuracy in treatment planning. By addressing these variables, ranging from material diversity to algorithmic synergy. Future studies can bridge the gap between phantom-based validation and routine clinical application.

Conclusion

iMAR algorithm reliably reduces metallic artifacts and improves HU and dose calculation accuracy, particularly under stringent gamma criteria, supporting its use for more precise EBRT planning in the presence of metallic implants.

References

1. Verburg JM, Seco J. CT metal artifact reduction methods: A quantitative comparison of commercial and non-commercial techniques. Med Phys. 2012;39: 4367–79.
2. Reft C, Alecu R, Das IJ, Gerbi JB, Keall P, Lief E, et al. Dosimetric considerations for patients with hip prostheses undergoing pelvic irradiation. Report of the AAPM Radiation Therapy Committee Task Group 63. Med Phys. 2003;30:1162–82.
3. Boas FE, Fleischmann D. CT artifacts: Causes and reduction techniques. Imaging Med. 2012;4:229–40.
4. Siemens Healthineers. Iterative Metal Artifact Reduction (iMAR): Technical principles and clinical applications. Siemens White Paper; 2015.
5. Meyer E, Raupach R, Lell M, Schmidt B, Kachelrieß M. Normalized metal artifact reduction (NMAR) in computed tomography. Med Phys. 2010;37: 5482–93.
6. Axente M, Paidi A, Von Eyben R, Hancock SL, Skinner L, Watkins WT, et al. Clinical evaluation of metal artifact reduction for CT-based radiotherapy planning. Phys Med Biol. 2015;60:4491–511.
7. Zhang Y, Huang J, Chen W, Chen J, Yan G, Lu J. Dosimetric evaluation of metal artifact reduction algorithms in radiotherapy planning using phantom studies. Phys Med. 2016;32: 235–43.
8. Mutic S, Palta JR, Butker EK, Das IJ, Huq MS, Loo LN, et al. Quality assurance for computed-tomography simulators and the computed-tomography-simulation process: Report of the AAPM Radiation Therapy Committee Task Group No. 66. Med Phys. 2003;30:2762-92.
9. Kalender WA, Hebel R, Ebersberger J. Reduction of CT artifacts caused by metallic implants. Radiology. 1987;164:576-7.
10. Maerz M, Koenig S, Schmitt D, Ackermann B, Ellerbrock M, Greilich S. Metal artifact reduction in CT imaging for radiotherapy planning: Dosimetric effects and clinical relevance. Phys Med Biol. 2016;61:N298-312.
11. Schmitt D, Maerz M, Koenig S, Ackermann B, Ellerbrock M, Greilich S. Impact of iterative metal artifact reduction on dose calculation accuracy in radiotherapy. Phys Med. 2021;82:1-8.